Available online at www.sciencedirect.com

jmr&t Journal of Materials Research and Technology

journal homepage: www.elsevier.com/locate/jmrt

Study on the durability of 3D printed calcium sulphoaluminate cement-based materials related to rheology control

Mingxu Chen [a], *Yuan Jin* [b], *Keke Sun* [c], *Shoude Wang* [b], *Piqi Zhao* [b], *Liang Wang* [a], *Junzhe Liu* [a,**], *Gongbing Yue* [a,*], *Qiuyi Li* [a], *Lingchao Lu* [b]

[a] College of Civil Engineering & Architecture, Qingdao Agricultural University, Qingdao 266109, China
[b] School of Material Science and Engineering, University of Jinan, Jinan 250022, China
[c] Department of Civil and Environmental Engineering, The Hong Kong Polytechnic University, Hong kong, China

ARTICLE INFO

Article history:
Received 5 June 2023
Accepted 8 August 2023
Available online 11 August 2023

Keywords:
Durability
3D printing
Thixotropy
Rheological properties
Radar map

ABSTRACT

Since 3D printed structure is conducted by the style of dimension reduction, the defects typically occur between the printing layers due to the poor rheological properties, which affects the durability most. This study focuses on exploring the durability of 3D printed calcium sulphoaluminate cement-based materials (CSACMs) with slag powder based on the correlation between printed structures and rheological parameters. Experimental results show that both the static and dynamic yield stress of 3D printed CSACMs exhibits a gradual increase with the slag powder content increases, while the thixotropy improves continually until reaching a maximum content at 15%. In this case, an increase in slag powder content leads to a significant reduction for structure deformation. However, poor printability occurs when the content of slag powder exceeds 15%. Besides, the chloride migration coefficient and maximum electric flux decreases from 7.28×10^{-12} to 3.27×10^{-12} m^2/s and 1347 to 711 K, respectively, when the content of slag powder increases from 0 to 10%. Meanwhile, the freezing resistance and linear shrinkage are improved. Based on the radar map correlation, structure deformation is significantly influenced by thixotropy, which is a crucial factor that can impact the durability of 3D printed CSACMs. In conclusion, the controllable rheology of 3D printed CSACMs are advantageous for improving the printed structures and durability.

1. Introduction

3D printing of building materials differs from traditional manufacturing methods in that it operates based on the digital 3D models and extrudes the cementitious material layer by layer through a nozzle [1–3]. 3D printing technology used for building materials can greatly reduce costs, save energy, and shorten the construction period [4,5], which is especially suitable for the preparation of special-shaped and functional decorative components or products with complex structures

* Corresponding author.
** Corresponding author.
E-mail addresses: liujunzhe@qau.edu.cn (J. Liu), yuegongbing@qau.edu.cn (G. Yue).
https://doi.org/10.1016/j.jmrt.2023.08.076

[6,7]. Meanwhile, it also can avoid the dust and construction waste pollution to realize the green manufacturing.

The stacking process of layer-by-layer manner is an inherent property of 3D printing, which realizes the structure build-up through converting the three-dimensional structure to two-dimensional structure [8–10]. Since 3D printing is conducted by the style of dimension reduction, the defects typically occur between the printing layers, and the performance loss is usually due to the formation of the weak surface, which affects the durability and structural stability most [11,12]. Recently, there remains some studies about the durability of 3D printed concrete or mortar. For instance, Baz et al. studied the resistance against sulfuric acid attacks of 3D printed concrete from a macro and micro scale, finding that the paste extrusion has a fundamental effect on the internal structure of printed materials, which extremely related to the durability [13]. Sun et al. studied mechanical properties and durability of 3D printed high-strength cementitious composites reinforced with PVA fibers, indicating that the durability of printed concrete was significantly affect by the occurred defects during the printing layers [14]. The current studies prove that the printed structural integrity and defects during the printing layers are the most significant factor in affecting the durability of 3D printed cement composites [15,16].

3D printing usually consists of three stages: pumping, extrusion, and stacking, which is the process from paste flow to rest [17,18]. Therefore, the printed structure and properties are related to the changes of flowability before and after the extrusion of paste, that is, excellent liquidity is needed to ensure the continuity of paste before extrusion and it needs to be hard enough to maintain its shape after extrusion [19,20]. To address this contradiction, it is essential to regulate rheological properties to construct stable printed sample with minimal structural deformation [21,22]. As studied by Souza et al., the effect of chemical admixtures on the correlation of rheology and buildability of 3D printed paste was investigated [23]. Recent studies have demonstrated that the rheological properties of paste can significantly impact the macro properties of 3D printed structure by controlling its stability, highlighting the crucial role of rheology in regulating the printed structure [24].

Despite the growing research on rheological parameters of 3D printed cement composites, there has been limited investigation into the correlation between these parameters, printed structures, and the durability. In this study, slag powder was introduced to enhance the durability of 3D printed CSACMs through controlling the rheological parameters and printed structure build-up. Dynamic and static yielding behaviors were obtained based on the shear-rate-controlled protocol, and the thixotropy of 3D printed CSACMs was evaluated using three-stage and creep-recovery curves protocol. In addition, the rapid chloride permeability coefficient, electric flux, freezing resistance, and linear shrinkage were investigated under different structure deformation. The radar map analysis was used to examine the relationships between rheological parameters, structural deformation, and durability, in order to identify the key factors that influence the durability of 3D printed CSACMs.

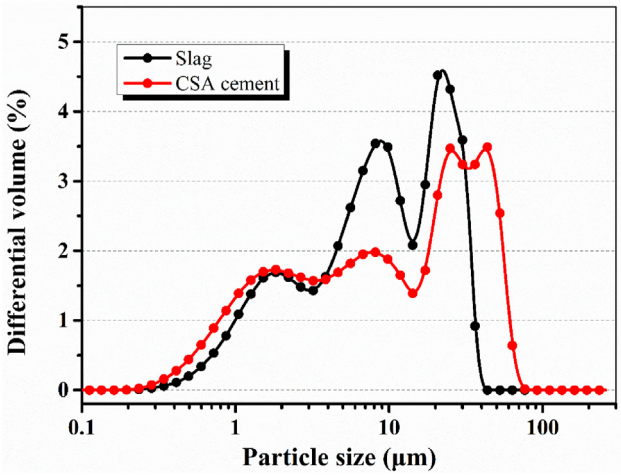

Fig. 1 – Particle size of CSA cement and slag powder.

2. Materials and method

2.1. *Raw materials*

Type R425 CSA cement was used in this study, which was provided by Zhonglian Cement Co., Ltd.; To reduce the viscosity and prevent the occurrence of "paste tailing", the quartz sand was utilized as fine aggregate; Hydroxypropyl methyl cellulose (HPMC) provided by the Heda Co., Ltd. was introduced to improve the bonding behaviors between the printing layers; Polycarboxylate superplasticizer provided by Shandong Academy of Building Research was incorporated to enhance the workability of printed paste; Tartaric acid (TA) was used to prolong the open time and improve the extrusion properties of printed paste; Bentonite was used as the thickener to improve the thixotropy and buildability of printed paste; Superfine slag powder was introduced to improve the durability of CSACMs. Table 1 and Fig. 1 presents the particle size and chemical compositions of CSA cement and slag powder, respectively.

Table 2 presents the mix design of 3D printed CSACMs, and the preparation procedures are outlined below. Firstly, the CSA cement, quartz sand, slag powder, HPMC and bentonite were blended in the V-shape blender (32 rpm); Secondly, the TA and superplasticizer were dissolved in water and then mixed with the solid mixture mentioned above for 5 min. Thirdly, the above mixtures was added into the 3D printer and

Table 1 – Chemical compositions of CSA cement and slag powder/%.

Components	CaO	Al_2O_3	SO_3	SiO_2	MgO	Fe_2O_3	TiO_2	K_2O	Na_2O	Others
CSA cement	45.82	21.94	18.03	9.00	1.87	1.82	0.99	0.30	–	0.23
Slag powder	40.55	14.75	2.92	29.12	9.41	0.45	0.61	0.45	1.07	0.67

Table 2 – Mix design of 3D printed CSACMs/%.

No.	CSA cement	HPMC	Superplasticizer	Sand	TA	Bentonite	Slag powder	Water
1	100	0.10	0.30	50	0.20	1	0	40
2	100	0.10	0.30	50	0.20	1	5	40
3	100	0.10	0.30	50	0.20	1	10	40
4	100	0.10	0.30	50	0.20	1	15	40
5	100	0.10	0.30	50	0.20	1	20	40

printed the samples according to the designed model; Finally, the printed sample was placed at room temperature to test the structure deformation until it unchanged within 10 min, and then the printed samples were cut to the tested shape by the standard mold.

2.2. 3D printer

A frame type 3D printer (JianYanHuaCe Science & Technology Co., Ltd.) is applied to construct the structures of 3D printed CSACMs, and the macro-structure of 3D printer is shown in Fig. 2, which includes operator panel, sliding axle, platform, and extrusion device. The nozzle diameter and printing speed is 10 mm and 60 mm/s, respectively. To test the durability and buildability better, the size of printed sample was fixed at 250 × 150 × 250 mm.

2.3. Testing methods

2.3.1. Rheological properties

The rheological properties were evaluated in this study by using a rotating rheometer (HAAKE MARS 40, Thermo Fisher Scientific, Germany) equipped with cylindrical rotor and plate–plate geometry. Thixotropy, yield stress, and creep and recovery were measured using shear-rate-controlled protocols. It should be noted that all rheological measurements were taken 5 min after the solid mixture contacts with the water.

(1) Dynamic yielding behaviors

The dynamic yield stress, plastic viscosity, and thixotropy was evaluated based on the shear-rate-controlled protocol. The paste was pre-sheared at a rate of 50 s^{-1} for 60 s, followed by a resting period of 120 s. The Dynamic yielding behaviors of the CSACMs were tested through subjecting a different shear rate ranging from 0 to 100 s^{-1} for a duration of 240 s. The tested and calculated shear rate are in the range of 0–100 s^{-1} and 10-90 s^{-1}, respectively, as shown in Fig. 3 (a). Recently, several models have been employed to characterize the dynamic yielding parameters of cementitious materials through calculating the fitting lines of down curves [25], as shown in Fig. 3 (b). The most commonly accepted model is the modified Bingham model, which is given by Eq. (1).

$$\tau = \tau_d + \mu\frac{d\gamma}{dt} + c\left(\frac{d\gamma}{dt}\right)^2 \quad (1)$$

where τ and τ_d represents the applied shear stress and dynamic yield stress, respectively; μ represents the plastic viscosity; $d\gamma/dt$ is the shear rate.

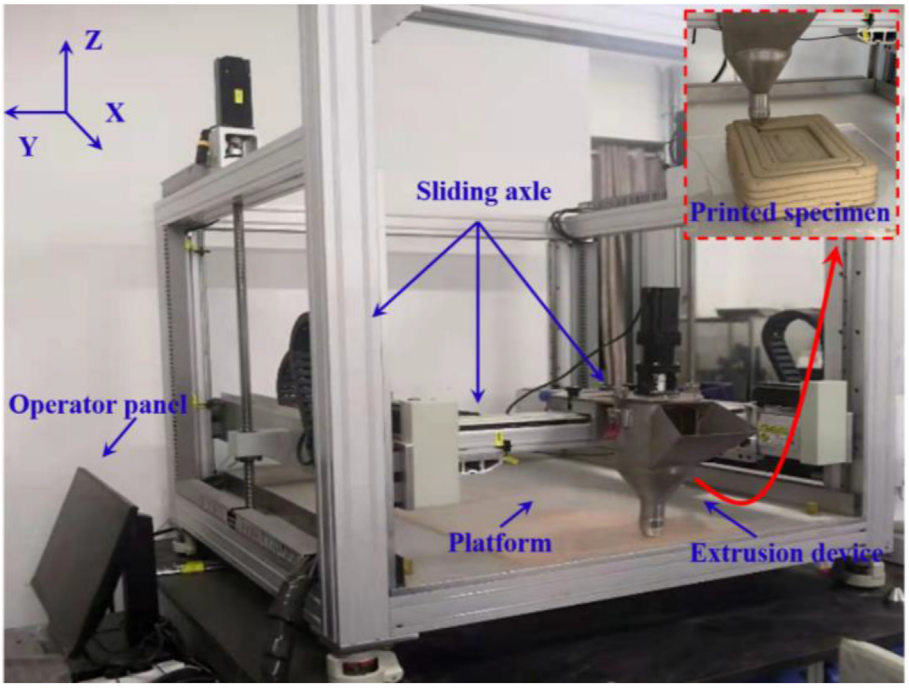

Fig. 2 – The structures of 3D printer.

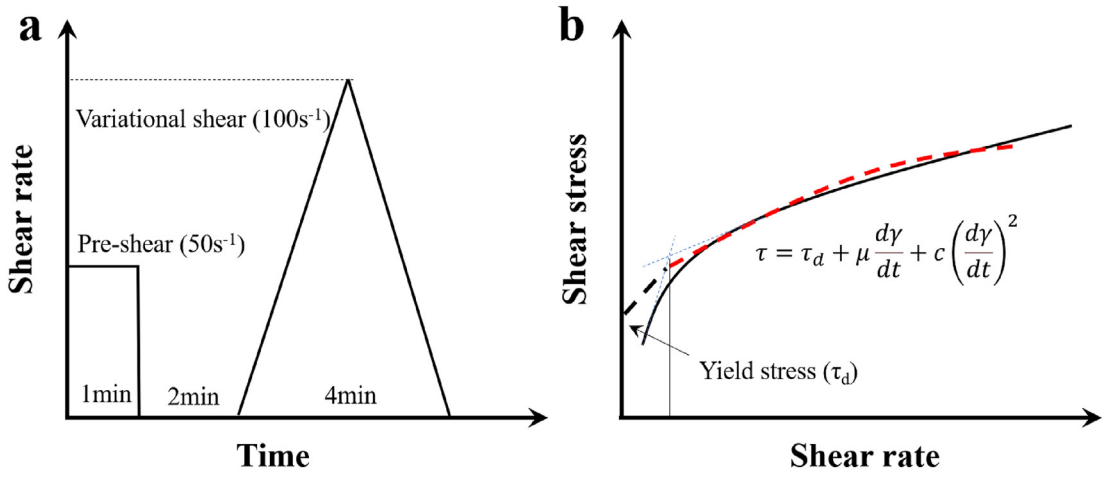

Fig. 3 – (a) Test procedures of shear-rate-controlled protocol; (b) the typical fitting line of dynamic yielding parameters calculated by the modified Bingham model.

(2) Static yielding behaviors

Static yielding behaviors were tested by the rotation shear protocol with a relative low shear rate to observe the state change of paste. The paste was first subjected to pre-shearing at a shear rate of 50 s^{-1} for 120 s, followed by a rest period of 10 min. Thereafter, a relative low shear rate of 0.1 s^{-1} was applied to test the shear stress variation, and continued for 60 s.

(3) Thixotropy

In addition, to examine the thixotropy of 3D printed CSACMs, the three-stage curve and creep-recovery protocols were employed. In Fig. 4 (a), three testing stage were conducted by different shear rate to monitor the recovery of apparent viscosity, and the applied shear rate were 0.1 s^{-1}, 100 s^{-1} and 0.1 s^{-1}, respectively. Low and high shear rate represent the static and dynamic state of paste, and the broken structures in the high shear rate can recover gradually at rest. High recovery degree means the better thixotropy and it can be expressed by Eq. (2).

$$R = \frac{\eta_1}{\eta_0} \times 100\% \quad (2)$$

where R is the recovery degree; η_0 and η_1 are the initial and recovery apparent viscosity.

The creep-recovery protocol is a measure that the ability of internal structure to resist slip deformation [26]. After applying a certain load (100 Pa) to the paste in the linear viscoelastic region, the strain decreases over time in the opposite direction of the creep extension when the load is removed, as shown in Fig. 4 (b). The recovery degree can used to investigate the thixotropy, and high recovery degree means the better thixotropy.

2.3.2. *Durability*

(1) Freeze-thaw resistance

The freeze-thaw resistance of 3D printed CSACMs was evaluated as per the standard GB/T 50082-2009. The 3D printed samples were cut into cube blocks with the size of 100 × 100 × 100 mm, and tested after curing for three days at

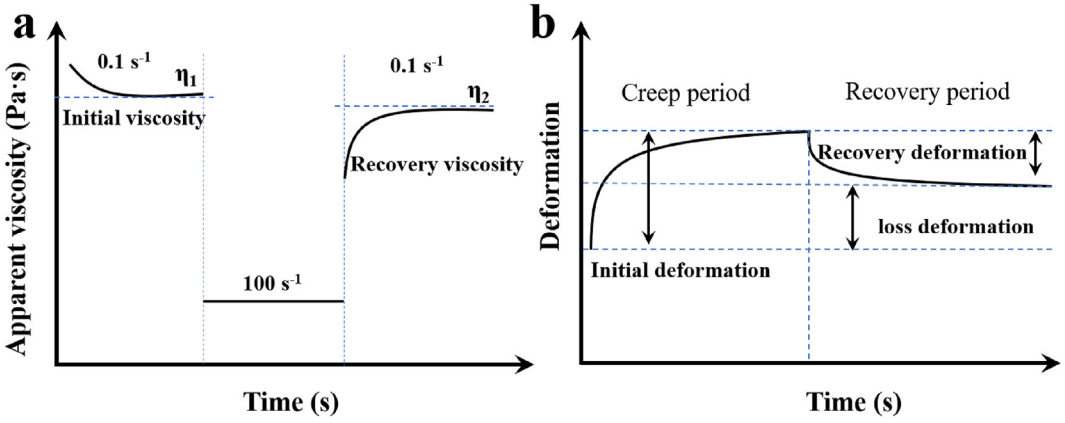

Fig. 4 – Typical curves of thixotropy: (a) three stage curves protocol and (b) creep and recovery protocol.

20 °C and 95% humidity. The mass loss and dynamic elastic modulus were recorded at cycle numbers of 0, 25, 50, 100, 200, 300, 400, 500 and 600, respectively.

(2) Rapid chloride migration (RCM) coefficient test

The cylindrical block with measuring 100 mm in diameter and 50 mm in height was used in RCM coefficient test which was tested after curing for three days at 20 °C and 95% humidity, respectively. Solution preparation: the deionized water was used to prepare the solution, and 10 wt.% NaCl and 0.3 mol/L NaOH solution was used as cathode electrolyte and anode electrolyte, respectively. After the test, the surface of sample is washed and dried, and the sample was cut in half axially using a cutting machine. The profile of the samples was sprayed with a prepared 0.1 mol/L silver nitrate solution to measure the penetration depth of the white chromogenic area, and the RCM coefficient was calculated according to the following equation Eq. (3).

$$D_{RCM} = \frac{0.0239 \times (273+T)L}{(U-2)t}\left(X_d - 0.0238\sqrt{\frac{(273+T)LX_d}{U-2}}\right) \quad (3)$$

where, D_{RCM} is the RCM coefficient, m^2/s; U is the voltage value, V; T is the average of initial and final temperatures, °C; L is the thickness of sample, mm; X_d is the average penetration depth, mm; t is the testing time, s.

(3) Rapid chloride permeability (RCP) test

The cylindrical block with measuring 100 mm in diameter and 50 mm in height was used in RCP test, which evaluated the permeability of 3D printed CSACMs accurately based on the measured electric flux. The electric flux of the sample was tested after curing for three days at 20 °C and 95% humidity, respectively. Solution preparation: the deionized water was used to prepare the solution, and 3 wt.% NaCl and 0.3 mol/L NaOH solution was used as cathode electrolyte and anode electrolyte, respectively. The sample was subjected to a 60 V potential between two chambers for a duration of 6 h. The current was measured and used to determine the total charge that passed through the sample.

(4) Linear shrinkage

The linear shrinkage of 3D printed samples was tested according to the standard ASTM C531-18. Firstly, The 3D printed samples were cut into cuboid blocks with dimensions of 40 × 40 × 160 mm and subsequently cured for 24 h at 20 °C and 95% humidity. Finally, the sample was transferred to a curing box with the temperature and humidity of 23 °C and 50%, respectively. The first test was performed using a length comparator before moving, and then the samples were tested every 6 h for the first three days and thereafter every 24 h. The calculation equation Eq. (4) of linear shrinkage is as follow.

$$S = [(L_0 - L)/L_0] \times 100\% \quad (4)$$

where, L_0 is the initial length, mm; L is the length after curing, mm.

2.3.3. Height variation and structure deformation

The buildability of 3D printed CSACMs was evaluated according to two parameters: the descent height and structure deformation. Height variation was evaluated based on the descent height, whereas the average deformation from three distinct directions was computed to determine the extent of structural deformation [27]. The calculated equation Eq. (5) of structure deformation is as follow.

$$D = \left(\frac{l-l_0}{3l_0} + \frac{w-w_0}{3w_0} + \frac{h_0-h}{3h_0}\right) \times 100\% \quad (5)$$

where D is the structure deformation; l_0, w_0, and h_0 represent the length, width, and height of printed model; l, w and h represent the length, width, and height of printed samples.

2.3.4. Porosity

A mercury intrusion porosimetry (Pore Master-60, USA) was applied to test the porosity of 3D printed CSACMs. The tested samples cured 3d were used in this experiment, and the tested pore diameters were in the range of 2 nm–400 nm.

3. Results and discussion

3.1. Rheological properties

By manipulating flow behavior of materials during printing, the rheology control can help prevent deformation or collapse of printed structures, resulting in more precise and consistent printing process [28]. Therefore, the controllable printed structure can be achieved through careful selection and adjustment of various parameters such as viscosity, elasticity, shear rate, yield stress, and thixotropy [29,30].

3.1.1. Dynamic yielding behaviors

The process of 3D printing is a paste flow process. In the extrusion or pumping stage, the paste is required to present well fluidity to achieve the excellent extrudability and continuity. In this case, it requires the low dynamic yielding properties to guarantee the flowability of paste [31]. Nonetheless, low dynamic yielding behaviors can lead to poor 3D printed structures, and high dynamic yield stress or plastic viscosity may cause the phenomenon of “paste tailing” or even nozzle blockage during extrusion [32]. Therefore, to achieve successful printing of the desired structure, a suitable dynamic yielding behavior is crucial. Fig. 5 presents shear stress curves of 3D printed CSACMs obtained by shear rate descending and growth protocol. Shear stress increases and decreases gradually with an increase and a decrease in shear rate, respectively. The descending shear stress increases sharply first due to the breakdown of flocculation structure and then increases linearly. Moreover, the addition of slag powder at contents ranging from 0 to 20% in the 3D printed CSACMs leads to an increase in shear stress. The modified Bingham model and fitting of descending shear stress curves were utilized to determine the dynamic yield stress and plastic viscosity, which considers the change of flocculation structure [33], as shown in Fig. 5 (a). The results in Fig. 5 (b) indicate that the dynamic yield stress and plastic viscosity increase gradually from 92.27 to 161.6 Pa and 5.56–10.96 Pa s,

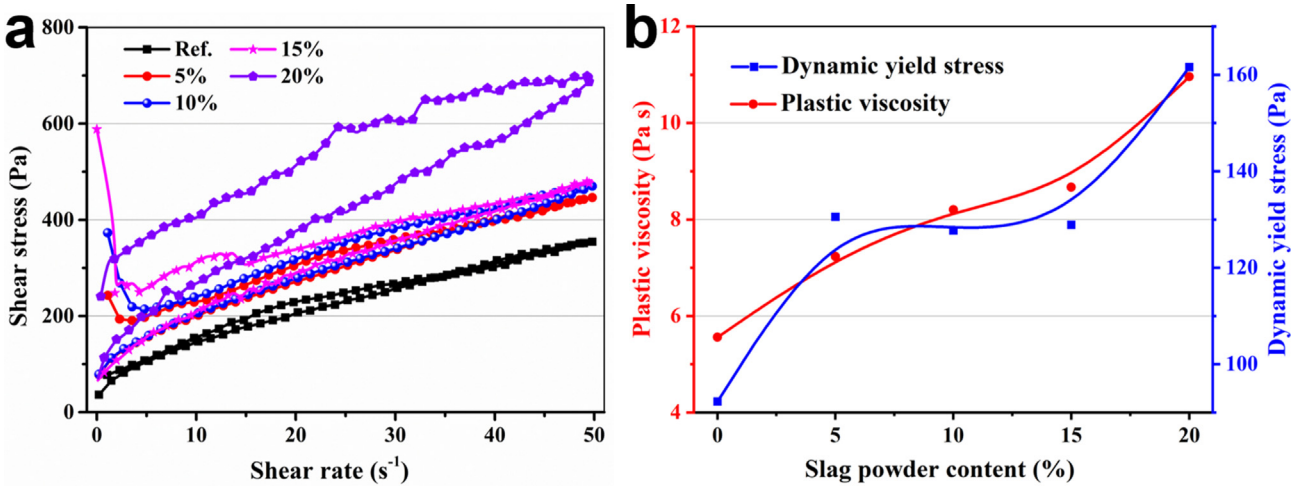

Fig. 5 – (a) Shear stress curves obtained by shear rate descending and growth protocol and (b) plastic viscosity and dynamic yield stress under different contents of slag powder.

respectively. The reason is that the slag powder absorbs free water existed in the printed paste, leading to an increase in internal friction.

3.1.2. *Static yield stress*

The process of paste stacking plays a crucial role in determining the stability of structural build-up and the improvement of its properties. The buildability of 3D printed paste during the stacking process is typically evaluated using static yield stress [34], which is obtained through the rotation shear protocol with a relatively low shear rate. In Fig. 6 (a), the shear stress changes over time in a relatively low shear rate of 0.1 s^{-1}, initially increasing sharply and then gradually decreasing until it reaches a relatively steady value. The maximum value of shear stress curve is indicative of static yield stress, which suggests a gradual flow of the printed paste due to microstructure failure. Furthermore, the static yield stress increases from 310 to 2472 Pa when slag powder contents increase from 0 to 20%, as shown in Fig. 6 (b), and it indicates that the introduction of slag powder is beneficial in resisting paste deformation and improve the buildability.

3.1.3. *Thixotropy*

Thixotropy is regarded as the rheological phenomenon characterized by the variation in viscosity over time in the presence of an external force [35]. As for the 3D printing materials, it should have the ability to flow easily from the nozzle. Nevertheless, the printed paste should quickly regain the stiffness after extrusion [36]. This process is known as thixotropy and is crucial in ensuring the successful of 3D printing. To compare the change of thixotropy of printed paste, the three-stage and creep-recovery curves based on shear-rate/stress-controlled protocol were used to investigate the thixotropy of 3D printed CSACMs. The three-stage curve simulates the thixotropy of the paste extrusion process, and the paste state of printed samples changes from static to dynamic. The three stage curves of 3D printed CSACMs shown in Fig. 7 (a) indicate that the apparent viscosity increases with the

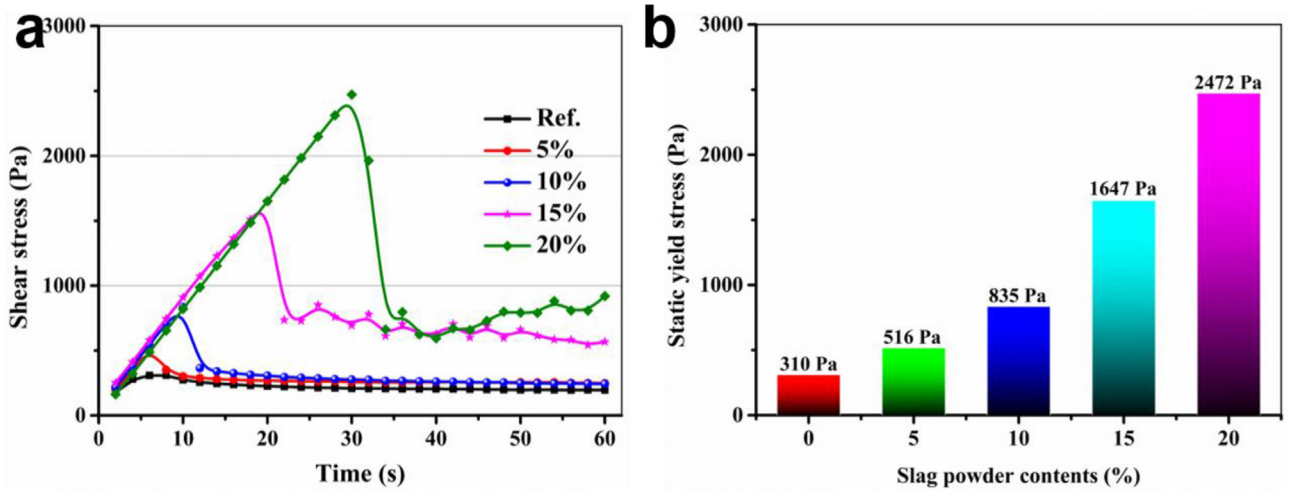

Fig. 6 – (a)The change in shear stress of 3D printed CSACMs over time in a relatively low shear rate and (b) the static yield stress changes with slag powder content.

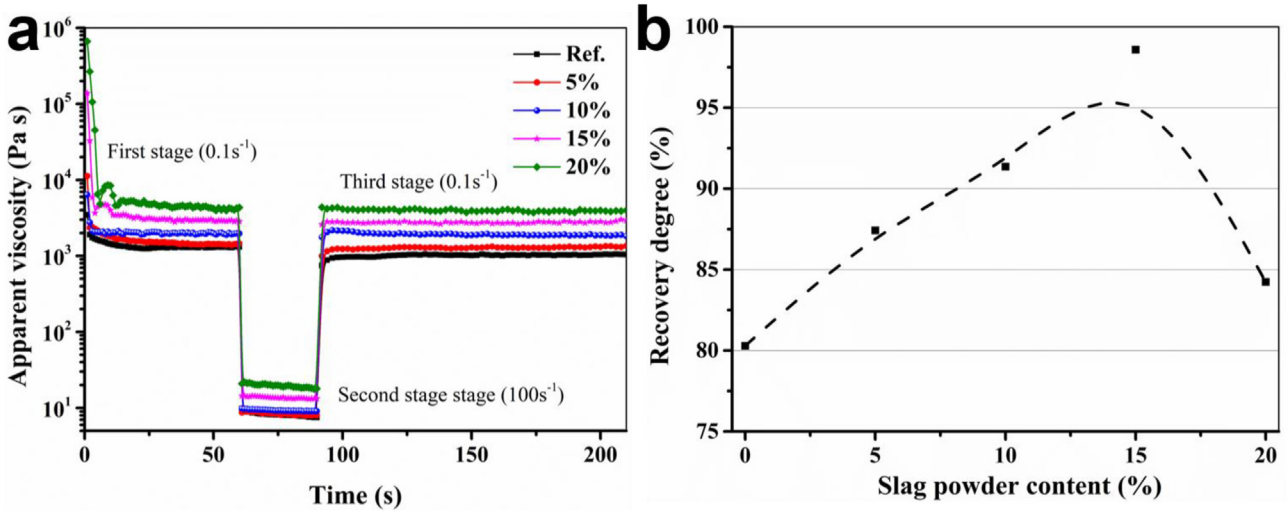

Fig. 7 – (a) Three stage curves change with time and (b) recovery degree under different slag powder contents.

increasing slag powder contents over time. According to Eq. (2), the recovery degree was obtained based on the first and third stage, and Fig. 7 (b) presents the recovery degree of 3D printed CSACMs increases until the slag powder content reaches 15%, which means the introduction of slag powder is beneficial for improving thixotropy. However, the recovery degree of 3D printed CSACMs decreases when the slag powder content exceeds 15%. Such a phenomenon is attributed to the recovery of viscosity caused by the break-down of paste microstructure [37]. Although the shear rate during the three-stage curve protocol is very small, it is still a dynamic change and exists the paste deformation [38]. The content of cementitious material in the printed paste decreases by adding slag powder. Therefore, to achieve the same dynamic change when the slag powder content exceeds a certain amount, it is necessary to break more paste microstructure that cannot be recovered in a short time, which causes the thixotropy to decline.

During the extrusion process, there remains a corresponding increase in both the weight and deformation as the build-up of printed structure layer by layer. This phenomenon is linked to creep, a gradual process that occurs over time [39]. To verify the validity of the thixotropy test, the creep protocol was introduced, which is almost no deformation during the linear viscoelastic region. Fig. 8 (a) shows the creep and recovery curves of 3D printed CSACMs, presenting that the compliance increases in a short time and then almost no change with time. In addition, the compliance decreases with the increasing contents of slag powder. This phenomenon means that the slag powder is in favor of the resistance of paste deformation. Fig. 8 (b) presents the recovery of paste deformation reaches the maximum value of 80% when the slag powder contents is 20%. Different with the three stage curves, the creep and recovery protocol can used to investigate the thixotropy of 3D printed CSACMs with high slag powder contents. The reason is that the three-stage curves

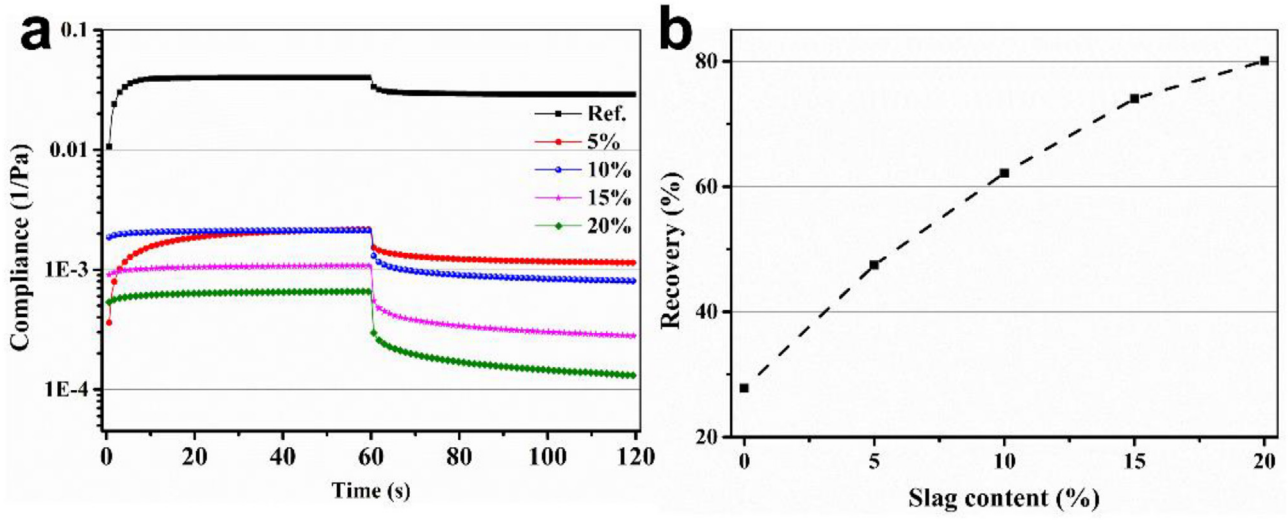

Fig. 8 – (a) Creep and recovery curves change with time and (b) recovery degree under different slag powder contents.

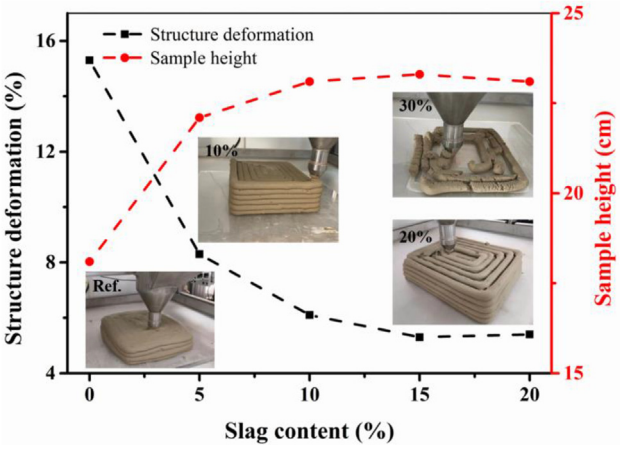

Fig. 9 – Structure deformation and sample height of 3D printed CSACMs.

protocol is to test thixotropy when the paste has a small fluidity, while the creep recovery method is based on the linear viscoelastic region without deformation. Therefore, once the viscosity or yield stress of the paste is too high, the three-stage method will remain certain errors.

The rheological properties of cementitious materials can be affected by the specific surface area and chemical activity of slag powder in both positive and negative ways. Based on the above results, the thixotropy of 3D printed CSACMs was improved for the following reasons: fine particles of slag powder have a micro-filling effect that benefits to release the entrapped water within cement particles, and the high specific surface area allows for the increased adsorption of superplasticizer. However, it is worth noting that the slag powder may require a larger amount of water compared to cement particles, which could potentially decrease the rheological properties. In this case, 3D printed CSACMs with high content of slag power will release a large amount of absorbed free water and superplasticizer in the shearing process, and it will be re-absorbed in the static process, resulting in significant changes in thixotropy. However, it should be noted that the thixotropy becomes poor once the content of slag powder exceeds the limit value.

3.2. *Structure deformation*

Achieving controllable rheology and high stiffness is advantageous for constructing printed structures, and improved buildability is a fundamental requirement for their practical applications [40,41]. As shown in Fig. 9(a) and (b), the deformation of printed structure exhibits a noticeable reduction with the increase of height of printed CSACMs and slag powder contents. Combined with the above rheological properties, the controllable rheology is advantageous in minimizing structure deformation, particularly with regards to thixotropy and yielding behaviors. From the macrograph of printed sample, there remains many cracks during the structures once the slag powder content exceeds 10%. The reason is that the extrusion of CSACMs from a 3D printer is challenging due to the occurrence of nozzle blockage [42], which suggests that high yield stress is detrimental to achieving optimal structure build-up.

3.3. *Correlation of rheological properties and structure deformation*

Effective rheology control plays a critical role in achieving optimal printing quality for a wide range of applications across industries. The rheological factors mentioned above have a significant impact on 3D printed structures. Fig. 10 (a) demonstrates a weak correlation between yield stress and structure deformation in 3D printed CSACMs, the main anomaly is due to high slag powder content. In contrast, Fig. 10 (a) depicts the relationship between thixotropy and structure deformation in 3D printed CSACMs. The results obtained from the creep and recovery protocol show a strong correlation between thixotropy and structure deformation, proving that the creep recovery method based on the linear viscoelastic region is accurate. Moreover, the structure deformation decreases considerably as the recovery degree increases, thus providing further evidence that improved thixotropy can effectively withstand deformation of printed

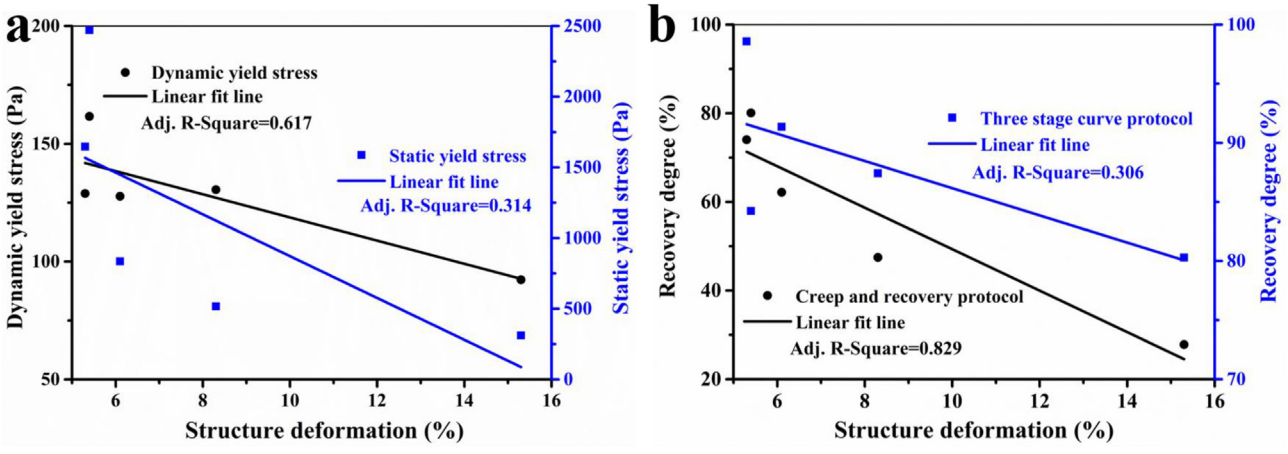

Fig. 10 – Correlation: (a) yield stress and structure deformation of 3D printed CSACMs (b) thixotropy and structure deformation of 3D printed CSACMs.

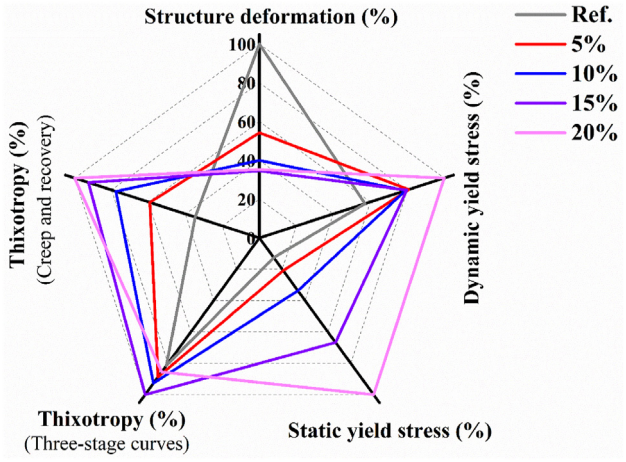

Fig. 11 – Radar map correlation of structure deformation and rheological properties.

structure. To illustrate the impact of different factors more clearly on structural deformation at various levels of slag powder content, a radar map diagram is employed, as shown in Fig. 11. The radar map method is a graphical representation that utilizes the maximum value of each factor to calculate the percentage conversion, which allows for the consideration of the interaction of multiple parameters. As shown, the variation in rheological parameters is closely linked to structure deformation, when the slag powder content is in the range of 0–15%. Beyond this range, particularly when the slag powder content reaches or exceeds 20%, the structure deformation reaches the limit value and no longer decreases and the rheological parameters cease to be direct factors affecting the structure deformation. In terms of change magnitude, the thixotropy has a greater impact on structure deformation than yield stress. The reason is that such a slight fluctuation in thixotropy can significantly affect structure deformation, highlighting its importance as a key influencing factor.

3.4. *Durability*

3.4.1. *Freezing resistance*

Freeze-thaw failure refers to the damage to the internal structure of cement-based materials caused by prolonged exposure to freeze-thaw cycles [43]. The damage of internal structure is primarily caused by the volume of the water inside the concrete changes in the process of freeze-thaw (water to ice), which causes fatigue stress in the concrete, leading to the structural damage. Fig. 12 illustrates the mass loss and dynamic elastic modulus of 3D printed CSACMs under varying numbers of freeze-thaw cycle, indicating that an overall downward trend in both the mass loss and dynamic elastic modulus occurs as the number of freeze-thaw cycles increases. Fig. 12(a) and (b) demonstrate that the mass loss and dynamic elastic modulus of 3D printed CSACMs exhibit improvement when the slag content is below 10%. Moreover, compared to the reference sample, the macroscopic cracks in

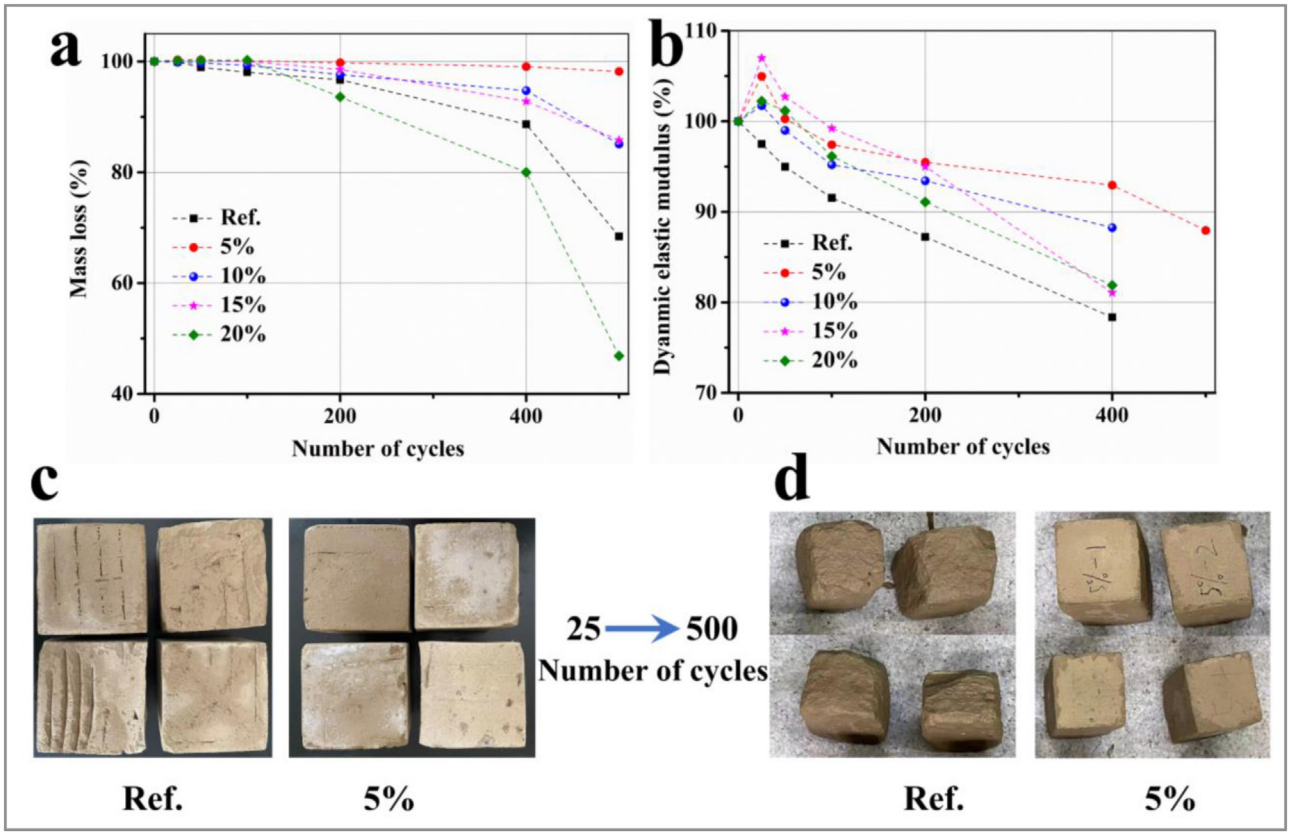

Fig. 12 – (a) The mass loss and (b) dynamic elastic modulus of 3D printed CSACMs under different number of cycles, and macrographs of 3D printed CSACMs under (c) 25 and (d) 500 times of freeze-thaw cycles.

3D printed CSACMs (Fig. 12(c) and (d)) decrease significantly as the number of freeze-thaw cycles increases. The reason is that the size of slag powder particles is comparatively smaller than that of cement particles, which leads to a reduction in the porosity of 3D printed CSACMs. Consequently, there is less free water exists in the 3D printed CSACMs, which reduces the chance from water to ice. However, the reverse phenomenon appears when the slag content is greater than 15%. The reason is that the addition of slag powder reduces the amount of cementitious material, resulting in the reduction of hydration products and poor compactness. Additionally, higher slag powder content can increase the yield stress (in Fig. 7), leading to the poor extrusion, which increases the macroscopic cracks in the paste. In this case, free water is more likely to enter the inside sample, leading to great damage in the process of freeze-thaw cycle.

3.4.2. *RCM coefficient*

The permeability of concrete will directly affect its durability (including frost resistance, impermeability, etc.), and the permeated height of chloride ions can be investigated by determining the RCM coefficient [44]. The macrographs of 3D printed CSACMs after chloride migration were shown in Fig. 13 (a)~(e), and RCM coefficient was calculated by the permeated height of chloride ions on the fracture surface. Fig. 13 (f) presents the RCM coefficient of 3D printed CSACMs under different contents of slag powder, indicating that the RCM coefficient initially decreased before increasing again with the increasing contents of slag powder. When the content of slag powder increases from 0 to 10%, the RCM coefficient reduces from 7.28 $\times$ 10^{-12} to 3.27 $\times$ 10^{-12} m^2/s, the permeability of 3D printed CSACMs was improved. In this case, the permeated height decreases gradually, as shown in Fig. 13 (a)~(c). The reason is that the size of slag powder particles is comparatively smaller than that of cement, leading to the reduction of porosity for 3D printed CSACMs, thus the dense structures delay the transmission of chloride ions. Therefore, the introduction of slag powder has a significant impact on the properties of 3D printed CSACMs. When the content exceeds 10%, the reduction of cementitious material becomes noticeable, resulting in the increase of macroscopic cracks and poor compactness, which is conducive to the transmission of chloride ion in the 3D printed CSACMs.

3.4.3. *Electric flux*

The RCP method utilizes the measured electric flux to evaluate the permeability of concrete accurately and efficiently [45]. In Fig. 14 (a), the electric flux of 3D printed CSACMs increases gradually over time. In addition, the maximum electric flux initially decreases from 1347 to 711 K and then increases with the increase of slag powder content, as shown in Fig. 14 (b), suggesting that the permeability of 3D printed CSACMs improves when the slag powder content is below 10%. The reason is that the content of cementitious material reduces due to the excessive content of slag powder, resulting in the decrease of hydration products and the failure of paste densification. Besides, excessive slag powder can cause poor printing performance of 3D printed CSACMs, and more visible cracks occurs in the printed sample, which increases the transmission probability of chloride ion within the paste.

3.4.4. *Linear shrinkage*

Linear shrinkage, primarily caused by water evaporation, is a critical indicator for assessing the long-term durability of cement-based materials. Fig. 15 shows the influence of slag powder on the linear shrinkage of 3D printed CSACMs, presenting that the linear shrinkage increases first and then decrease with the increase of time. The increase of linear shrinkage occurred before 7 d, which was mainly caused by the rapid hydration of CSA cement in the early stage. In addition, the linear shrinkage decreases significantly when the content of slag powder is less than 10%. The reason is that the size of slag powder particles is comparatively smaller than that of cement particles, resulting in the increase of compactness and the reduction of free water. As the proportion of slag powder in the mixture exceeds 10%, there remains a gradual increase in linear shrinkage, which was attributed to an excessive amount of slag powder. At the same time, excessive slag powder can negatively impact the printing performance of the paste, leading to an increased occurrence

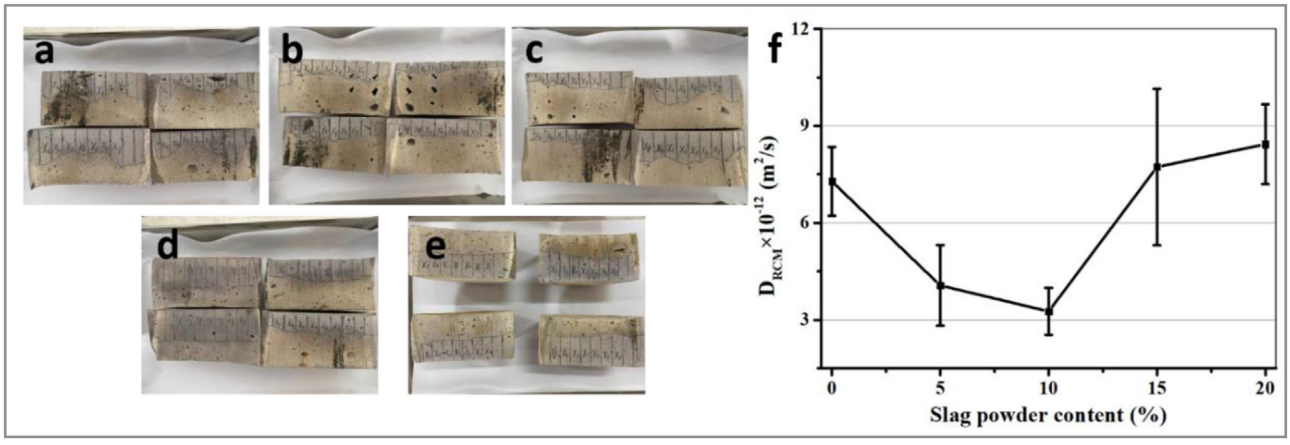

Fig. 13 – Macrographs of 3D printed CSACMs after chloride migration: (a) Ref., (b) 5% slag powder, (c) 10% slag powder, (d) 15% slag powder, (e) 20% slag powder; (f) RCM coefficient of 3D printed CSACMs.

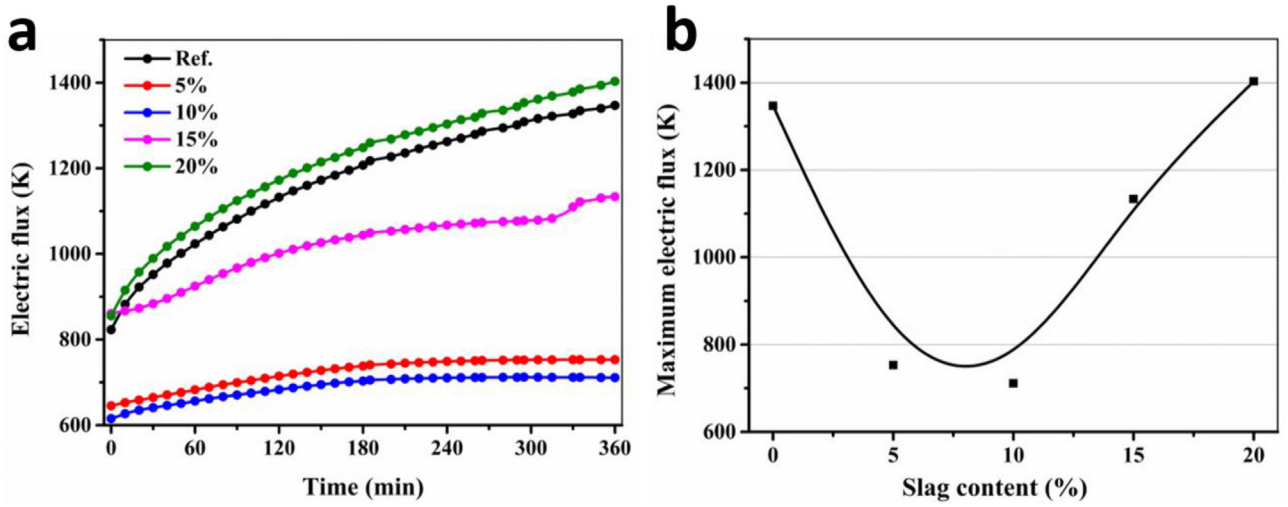

Fig. 14 – (a) The electric flux of 3D printed CSACMs with different contents of slag powder, and (b) calculated maximum electric flux of 3D printed CSACMs.

of macroscopic cracks within the material [45]. Additionally, it can also cause a deterioration in bonding properties between printed layers and facilitate entry of free water into the structure.

3.5. *Correlation of durability and structure deformation*

To explore the influence of structural deformation on the durability, the correlation was evaluated by radar map, as shown in Fig. 16. The structure deformation decreases gradually and the durability improves when the slag contents increase from 0 to 10%. Moreover, when slag powder contents exceed 10%, even minor fluctuations in structure deformation can significantly impact the durability of CSACMs. This phenomenon is due to the challenge of extruding CSACMs from 3D printers, which are prone to nozzle blockage. Although it presents smaller structure deformation, many macro-cracks occur due to the poor rheological properties, which will provide erosion channels for water or ions. Although structure deformation significantly affects durability, it shows a trend of initial improvement and subsequent deterioration with an increase in slag powder content or a decrease in structure deformation. Several factors contribute to this phenomenon. For instance, there also remains an indirect relationship between rheological properties and durability. The successful stacking of 3D printed cementitious materials primarily relies on its extrudability and pumpability, which is determined by rheological properties. Many references have proved that controllable rheological properties are beneficial to structural deformation or printing accuracy. Once the rheological properties become poor, the defects or interconnected pores typically occur between the printing layers due to nozzle blockage, which affects the durability and structural stability most. The rough and porous nature of printed sample will provide the channel for the ion or water and cause high capillary water absorption of the outer layer [46]. The presence of

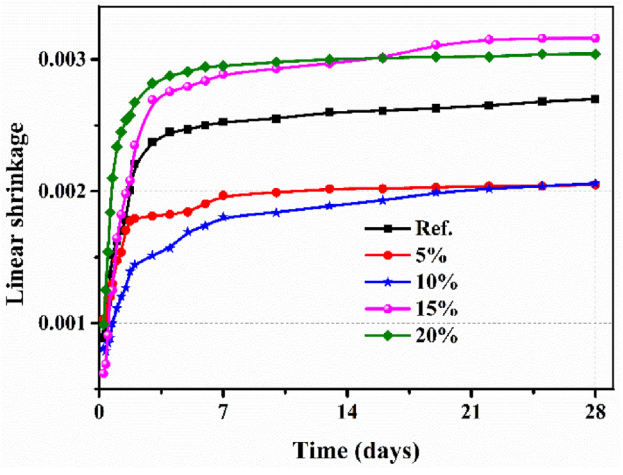

Fig. 15 – Linear shrinkage of 3D printed CSACMs with slag powder.

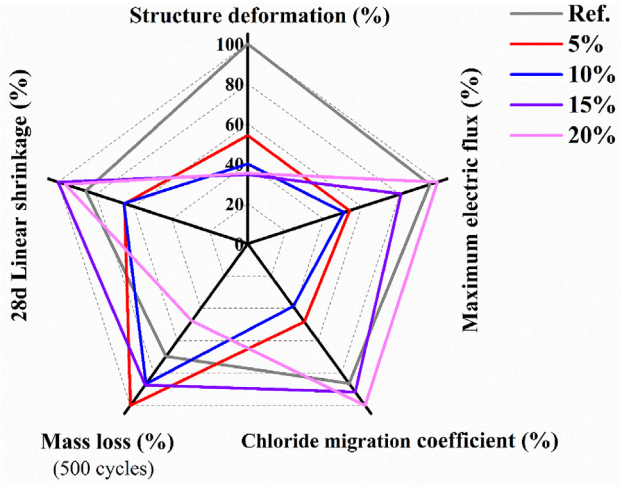

Fig. 16 – Radar map correlation of structure deformation and durability of 3D printed CSACMs.

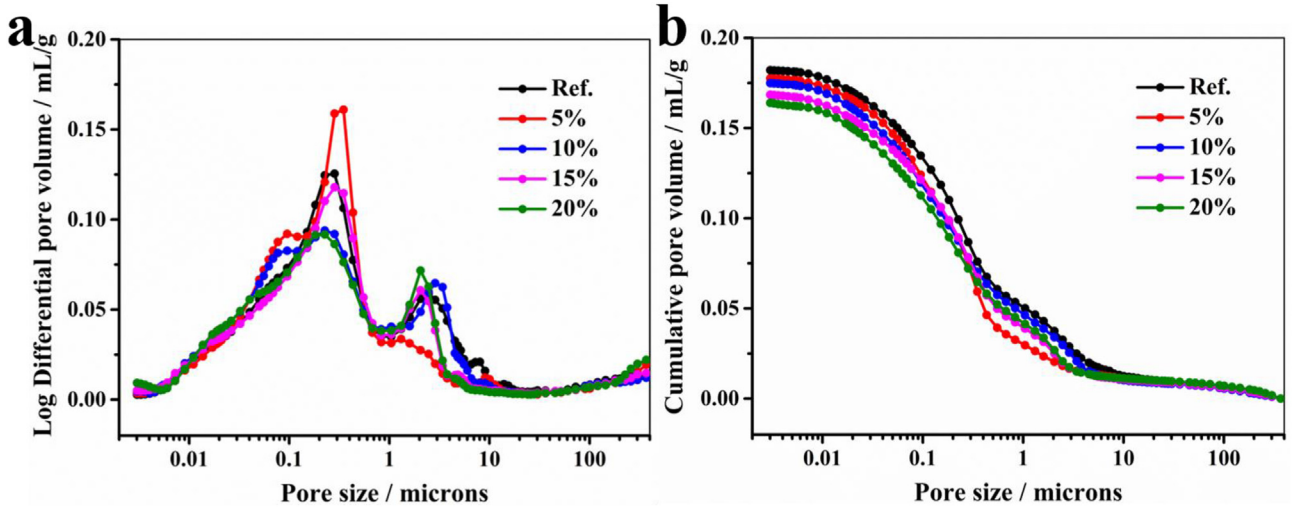

Fig. 17 – Porosity of 3D printed CSACMs: (a) differential pore volume and (b) cumulative pore volume.

interconnected pores at the interface amplifies the vulnerability of printed materials to durability [11]. Additionally, the rheology of printed paste influences the porosity at the layer interface. When the printed paste has a higher yield stress and elastic modulus, it becomes more rigid and stiffness, making it difficult for successive printing layer and thus leading to increased porosity [47]. When the printed structure starts to present deformation, the rheological properties of paste improve, and the interlayer structure becomes relatively dense. At this time, the durability of printed sample is closely related to the porosity. As shown in Fig. 17(a) and (b), the porosity of 3D printed CSACMs decreases gradually with the increase of slag powder contents, indicating that the introduction of slag powder is beneficial to improve the compactness. Compare with the influence of microscopic pores, the defects or macro pores caused by interlayer structures have a dominant influence on the durability when the slag powder content is higher than 10%, as a result, such samples tend to exhibit poorer durability.

4. Conclusions

In this study, the slag powder is utilized to control the rheological parameters of 3D printed calcium sulphoaluminate cement-based materials (CSACMs), thereby improving printed structure accurately and controlling the durability. The potential for developing 3D printed CSACMs with excellent shape retention and durability is significant through controlling the rheology. The main conclusions of this study can be summarized as follows.

(1) The static and dynamic yield stress increases from 92.27 to 161.6 Pa and 310–2472 Pa, respectively, with the slag powder content increases from 0 to 20%.
(2) According to the creep-recovery, and the three stage curves protocol, the thixotropy is improved until the slag powder content reaches 15%.
(3) The structure deformation of 3D printed CSACMs deceases significantly as the content of slag powder increases. However, poor printability occurs when the content of slag powder exceeds 15%.
(4) The RCM coefficient and maximum electric flux decreases from 7.28×10^{-12} to 3.27×10^{-12} m^2/s and 1347 to 711 K, respectively, with an increase in slag powder content from 0 to 10%. Meanwhile, the freezing resistance and linear shrinkage are improved.
(5) Based on the radar map correlation, the thixotropy is a key factor influencing structure deformation which affects the durability obviously.

Declaration of Competing Interest

There are no conflicts of interest to this work.

Acknowledgments

This research was funded by the Natural Science Foundation of Shandong Province (ZR202111220187 and ZR2020ME036), Top Talent Program of Qingdao Agricultural University (6651122007), Natural Science Foundations of China (51778302 and 52072147) and School-enterprise Project (20213702032890).

REFERENCES

[1] Jiang Q, Liu Q, Wu S, Zheng H, Sun W. Modification effect of nanosilica and polypropylene fiber for extrusion-based 3D printing concrete: printability and mechanical anisotropy. Addit Manuf 2022;56:102944.
[2] Xu Z, Zhang D, Li H, Sun X, Zhao K, Wang Y. Effect of FA and GGBFS on compressive strength, rheology, and printing properties of cement-based 3D printing material. Construct Build Mater 2022;339:127685.
[3] Shakor P, Nejadi S, Paul G, Gowripalan N. Effects of different orientation angle, size, surface roughness, and heat curing on mechanical behavior of 3D printed cement mortar with/

without glass fiber in powder-based 3DP. 3D Print Addit Manuf 2023;10(2):330–55.
[4] Xiao J, Ji G, Zhang Y, Ma G, Mechtcherine V, Pan J, et al. Large-scale 3D printing concrete technology: current status and future opportunities. Cem Concr Compos 2021;122:104115.
[5] De Schutter G, Lesage K, Mechtcherine V, Nerella VN, Habert G, Agusti-Juan I. Vision of 3D printing with concrete—technical, economic and environmental potentials. Cement Concr Res 2018;112:25–36.
[6] Zhang J, Wang J, Dong S, Yu X, Han B. A review of the current progress and application of 3D printed concrete. Compos. Part A-Appl S 2019;125:105533.
[7] Han Y, Yang Z, Ding T, Xiao J. Environmental and economic assessment on 3D printed buildings with recycled concrete. J Clean Prod 2021;278:123884.
[8] Lee JH, Kim JH. Matric suction of fine sand and its effect on the shape stability of 3D printed cement mortar. Construct Build Mater 2022;341:127618.
[9] Mohan MK, Rahul A, De Schutter G, Van Tittelboom K. Extrusion-based concrete 3D printing from a material perspective: a state-of-the-art review. Cem Concr Compos 2021;115:103855.
[10] Lin A, Goel A, Yeo C, Chung J, Dai Pang S, Wang C-H, et al. Compressive load-dominated concrete structures for customized 3D-printing fabrication. Autom ConStruct 2022;141:104467.
[11] Zhang Y, Zhang Y, Yang L, Liu G, Chen Y, Yu S, et al. Hardened properties and durability of large-scale 3D printed cement-based materials. Mater Struct 2021;54:1–14.
[12] Nodehi M, Aguayo F, Nodehi SE, Gholampour A, Ozbakkaloglu T, Gencel O. Durability properties of 3D printed concrete (3DPC). Autom ConStruct 2022;142:104479.
[13] Baz B, Aouad G, Kleib J, Bulteel D, Remond S. Durability assessment and microstructural analysis of 3D printed concrete exposed to sulfuric acid environments. Construct Build Mater 2021;290:123220.
[14] Sun X, Zhou J, Wang Q, Shi J, Wang H. PVA fibre reinforced high-strength cementitious composite for 3D printing: mechanical properties and durability. Addit Manuf 2022;49:102500.
[15] Wang L, Ma H, Li Z, Ma G, Guan J. Cementitious composites blending with high belite sulfoaluminate and medium-heat Portland cements for largescale 3D printing. Addit Manuf 2021;46:102189.
[16] Surehali S, Tripathi A, Nimbalkar AS, Neithalath N. Anisotropic chloride transport in 3D printed concrete and its dependence on layer height and interface types. Addit Manuf 2023:103405.
[17] Wu Y, Liu C, Liu H, Zhang Z, He C, Liu S, et al. Study on the rheology and buildability of 3D printed concrete with recycled coarse aggregates. J Build Eng 2021;42:103030.
[18] Arunothayan AR, Nematollahi B, Khayat KH, Ramesh A, Sanjayan JG. Rheological characterization of ultra-high performance concrete for 3D printing. Cem Concr Compos 2023;136:104854.
[19] Jacquet Y, Perrot A, Picandet V. Assessment of asymmetrical rheological behavior of cementitious material for 3D printing application. Cement Concr Res 2021;140:106305.
[20] Jiao D, Shi C, De Schutter G. Magneto-rheology control in 3D concrete printing: a rheological attempt. Mater Lett 2022;309:131374.
[21] Sanjayan J, Jayathilakage R, Rajeev P. Vibration induced active rheology control for 3D concrete printing. Cement Concr Res 2021;140:106293.
[22] Zhao Z, Chen M, Jin Y, Lu L, Li L. Rheology control towards 3D printed magnesium potassium phosphate cement composites. Compos. Part B-Eng 2022;239:109963.
[23] Souza MT, Ferreira IM, de Moraes EG, Senff L, de Oliveira APN. 3D printed concrete for large-scale buildings: an overview of rheology, printing parameters, chemical admixtures, reinforcements, and economic and environmental prospects. J Build Eng 2020;32:101833.
[24] Chen M, Li H, Yang L, Wang S, Zhao P, Huang Y, et al. Rheology and shape stability control of 3D printed calcium sulphoaluminate cement composites containing paper milling sludge. Addit Manuf 2022;54:102781.
[25] Chen M, Li L, Zheng Y, Zhao P, Lu L, Cheng X. Rheological and mechanical properties of admixtures modified 3D printing sulphoaluminate cementitious materials. Construct Build Mater 2018;189:601–11.
[26] Qian Y, Kawashima S. Use of creep recovery protocol to measure static yield stress and structural rebuilding of fresh cement pastes. Cement Concr Res 2016;90:73–9.
[27] Jin Y, Xu J, Li Y, Zhao Z, Chen M, Lu L, et al. Rheological properties, shape stability and compressive strength of 3D printed colored cement composites modified by needle-like pigment. Addit Manuf 2022;57:102965.
[28] Yao H, Xie Z, Li Z, Huang C, Yuan Q, Zheng X. The relationship between the rheological behavior and interlayer bonding properties of 3D printing cementitious materials with the addition of attapulgite. Construct Build Mater 2022;316:125809.
[29] Panda B, Sonat C, Yang E-H, Tan MJ, Unluer C. Use of magnesium-silicate-hydrate (MSH) cement mixes in 3D printing applications. Cem Concr Compos 2021;117:103901.
[30] Chen Y, Liu C, Cao R, Chen C, Mechtcherine V, Zhang Y. Systematical investigation of rheological performance regarding 3D printing process for alkali-activated materials: effect of precursor nature. Cem Concr Compos 2022;128:104450.
[31] Tay YWD, Qian Y, Tan MJ. Printability region for 3D concrete printing using slump and slump flow test. Compos. Part B-Eng 2019;174:106968.
[32] Xu J, Chen M, Zhao Z, Li L, Wang S, Huang Y, et al. Printability and efflorescence control of admixtures modified 3D printed white Portland cement-based materials based on the response surface methodology. J Build Eng 2021;38:102208.
[33] Jiao D, Shi C, Yuan Q, An X, Liu Y, Li H. Effect of constituents on rheological properties of fresh concrete-A review. Cem Concr Compos 2017;83:146–59.
[34] Yuan Q, Li Z, Zhou D, Huang T, Huang H, Jiao D, et al. A feasible method for measuring the buildability of fresh 3D printing mortar. Construct Build Mater 2019;227:116600.
[35] Chen M, Yang L, Zheng Y, Huang Y, Li L, Zhao P, et al. Yield stress and thixotropy control of 3D-printed calcium sulfoaluminate cement composites with metakaolin related to structural build-up. Construct Build Mater 2020;252:119090.
[36] Ding T, Xiao J, Zou S, Yu J. Flexural properties of 3D printed fibre-reinforced concrete with recycled sand. Construct Build Mater 2021;288:123077.
[37] Liang S, Wei Y. Effects of water-to-cement ratio and curing age on microscopic creep and creep recovery of hardened cement pastes by microindentation. Cem Concr Compos 2020;113:103619.
[38] Feng K, Xu Z, Zhang W, Shen J, Hu M, Long G, et al. Experimental study on dynamic and static structure establishment and recovery rate of fresh cement paste by composite thickening agents. Construct Build Mater 2022;343:128120.
[39] Chen M, Liu B, Li L, Cao L, Huang Y, Wang S, et al. Rheological parameters, thixotropy and creep of 3D-printed calcium sulfoaluminate cement composites modified by bentonite. Compos. Part B-Eng 2020;186:107821.

[40] Long W, Tao J, Lin C, Gu Y, Mei L, Duan H, et al. Rheology and buildability of sustainable cement-based composites containing micro-crystalline cellulose for 3D-printing. J Clean Prod 2019;239:118054.
[41] Muthukrishnan S, Ramakrishnan S. J. Sanjayan. Technologies for improving buildability in 3D concrete printing. Cem Concr Compos 2021;122:104144.
[42] Yang L, Sepasgozar SM, Shirowzhan S, Kashani A, Edwards D. Nozzle criteria for enhancing extrudability, buildability and interlayer bonding in 3D printing concrete. Autom ConStruct 2023;146:104671.
[43] Zhao Y, Wang L, Lei Z, Han X, Shi J. Study on bending damage and failure of basalt fiber reinforced concrete under freeze-thaw cycles. Construct Build Mater 2018;163:460–70.
[44] Yang L, Zhao P, Liang C, Chen M, Niu L, Xu J, et al. Characterization and adaptability of layered double hydroxides in cement paste. Appl Clay Sci 2021;211:106197.
[45] Moelich G, Kruger P, Combrinck R. Mitigating early age cracking in 3D printed concrete using fibres, superabsorbent polymers, shrinkage reducing admixtures, B-CSA cement and curing measures. Cement Concr Res 2022;159:106862.
[46] Rehman AU, Kim JH. 3D concrete printing: a systematic review of rheology, mix designs, mechanical, microstructural, and durability characteristics. Materials 2021;14:3800.
[47] Geng Z, She W, Zuo W, Lyu K, Pan H, Zhang Y, et al. Layer-interface properties in 3D printed concrete: dual hierarchical structure and micromechanical characterization. Cement Concr Res 2020;138:106220.